JOURNAL OF SOLID STATE CHEMISTRY 111, 75–82 (1994)

Determination of the Commensurately Modulated Structure of $NbGe_{2/5}Te_2$ from Twinned-Crystal Data

A. van der Lee,[1] M Evain, M. Mansuetto,[2] L. Monconduit, R. Brec, and J. Rouxel

IMN, Laboratoire de Chimie des Solides, 2, Rue de la Houssinière, 44072 Nantes Cedex 03, France

Received October 27, 1993; in revised form February 4, 1994; accepted February 7, 1994

IN HONOR OF C. N. R. RAO ON HIS 60TH BIRTHDAY

The commensurate modulation of the $NbGe_{2/5}Te_2$ structure has been determined from X-ray diffraction data collected on a twinned crystal. The (3 + 1)D superspace group is $P2_1/n(0\beta\gamma)$, $\beta = 0.0$, $\gamma = 0.4$. The basic unit cell dimensions are $a = 6.4437(9)$, $b = 16.004(2)$, $c = 3.8936(4)$ Å, $\alpha = 119.10(1)^\circ$, $V = 350.85(7)$ Å^3, and $Z = 4$. Final R factors are 0.051, 0.122, 0.187, and 0.110 for 742 main reflections, 1573 first-order superreflections, 927 second-order superreflections, and the combined set, respectively. Twinning is taken into account by an extra basic vector; the intensities of all reflections, overlapping as well as non-overlapping, are used in the final refinement. The twin volume ratio is refined to $\nu \approx 0.418(1)$. $NbGe_{2/5}Te_2$ is a layered compound consisting of [Te/Nb, Ge/Te] sandwiches with a close to orthorhombic basic structure modulated by strong monoclinic, commensurate occupational and displacive waves. Bond distances in the structure of $NbGe_{2/5}Te_2$ compare very well with those in the three- and seven-fold orthorhombic superstructures of $NbGe_{1/3}Te_2$ and $NbGe_{3/7}Te_2$, respectively. It is shown that all three structures are built from the same intrasandwich subunits, and that the stacking, and accordingly the 3D symmetry, is determined by the subunit geometry. The pinning of two sandwiches on each other is related to a few short intersandwich Te–Te contacts that in turn can be correlated to the electronic stabilization of the compound.

INTRODUCTION

Recent investigations in the phase diagram of M–A–Te (M = Nb, Ta; A = Si, Ge) have shown that MA_xTe_2 ($1/3 \leq x \leq 1/2$) compounds are characterized by a strong occupational modulation wave of both M and A occurring along with important displacive modulation waves of all atoms (*1, 2*). The structures are built from infinite two-dimensional [Te/M, A/Te] sandwiches, separated by empty Van der Waals gaps.

Research on the MA_xTe_2 tieline of the M–A–Te phase diagram is of interest, because it allows subtle changes to be monitored in the electronic structure versus changes in the geometric structure quite easily. Since oxidation states of 3+ and 2+ can be assigned to M and A (3), respectively, the mean oxidation state of Te has to be $-(3 + x)/2$. The latter oxidation state gives rise to an electronic transfer from Te p orbitals to M metal d-block bands (4). Fairly short intersandwich Te–Te contacts have been correlated to this electronic transfer.

The structural variation due to a variation of x is expressed in a variation of the magnitude of the modulation wave vector, since it can be shown that $\mathbf{q} = \gamma\mathbf{c}^* = x\mathbf{c}^*$ (1). x may take either rational values, leading to superstructures commensurate with the basic unit cell, or irrational values, yielding incommensurate structures with symmetry that cannot be described by an ordinary 3D space group. It should be noted that all structures are fully ordered, despite the use of (ir)rational values for x in MA_xTe_2. It was recently shown that (3 + 1)D superspace groups are suitable for a unified description of both commensurate and incommensurate structures in the MA_xTe_2 series (2).

Three different commensurate superstructures have been reported, viz. $NbSi_{1/2}Te_2$ (5); $MA_{1/3}Te_2$ with M = Nb, A = Ge (6, 7), M = Nb, A = Si (8), and M = Ta, A = Si (3); and $NbGe_{3/7}Te_2$ (2). One incommensurate structure has been determined, viz. $TaSi_{0.360}Te_2$ (1). All compounds, except $NbSi_{1/2}Te_2$, share the same (super)space group, viz. $Pnma(00\gamma)s00$. Apart from structure determinations, other investigations have been made, including band structure calculations (4), Scanning Tunneling Microscopy (STM) and Atomic Force Microscopy (AFM) imaging (9), and Li- and Na-intercalation experiments (10).

The compound which is the subject of this paper, $NbGe_{2/5}Te_2$, is different from all known orthorhombic MA_xTe_2 compounds, since the modulation wave has a clear monoclinic symmetry, whereas the basic structure

[1] To whom correspondence should be addressed.

[2] On leave from Department of Chemistry, Northwestern University, Evanston, Illinois 60208-3113.

0022-4596/94 $6.00

remains very close to orthorhombic. The nature of the monoclinic modulation in $NbGe_{2/5}Te_2$ will be discussed, along with the relation with the other phases in the MA_xTe_2 series.

EXPERIMENT

Numerous crystals of $NbGe_{2/5}Te_2$ were found in the batch that was obtained for the synthesis of $NbGe_{1/3}Te_2$ (7). A similar synthesis with the elements weighted in the proper ratios was performed (the heating scheme was several hours at 700 K, 2 days at 900 K, 2 days at 1100 K, 10 days at 1280 K, followed by quenching to air). SEM analysis, using $CrGeTe_3$ as internal standard for Ge, yielded the composition $Nb_{29}Ge_{12}Te_{60}$. Analysis by Weissenberg photographs showed a fairly complicated diffraction pattern in the b^*, c^* plane. However, a basic lattice consisting of strong spots could be identified with cell parameters very close to those of the $NbGe_{1/3}Te_2$ basic lattice. The metric symmetry of the basic unit cell is, within experimental error, orthorhombic. The weaker reflections could be indexed with two **q** vectors (Fig. 1),

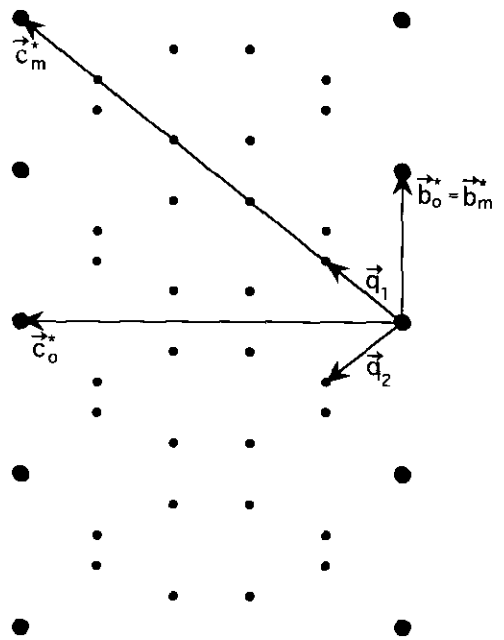

FIG. 1. Diffraction pattern of $NbGe_{2/5}Te_2$ in the $\mathbf{b}^*$, $\mathbf{c}^*$ plane.

$$\mathbf{q}_1 = \tfrac{2}{5}\,\mathbf{b}_o^* + \tfrac{1}{5}\mathbf{c}_o^* \quad [1]$$

$$\mathbf{q}_2 = -\tfrac{2}{5}\,\mathbf{b}_o^* + \tfrac{1}{5}\mathbf{c}_o^*. \quad [2]$$

Data collection of the main reflections and of the weaker satellite reflections (related to the main ones through Eqs. [1] and [2]) was performed on a SIEMENS-P4 diffractometer (see Table 1 for the recording conditions). The measured intensities were corrected for scale variation and Lorentz-polarization effects. A Gaussian absorption correction was applied using the ABSORB program from the XTAL system software (11). Symmetry-related reflections were averaged according to Laue symmetry $2/m11$ (vide infra), yielding an internal consistency factor based upon observed reflections of $R_i = 0.053$. A final number of 742 main reflections, 1573 first-order satellites, and 927 second-order reflections with intensities $I > 2.5\sigma(I)$ were available for the refinements.

TABLE 1
Crystal Data of $NbGe_{2/5}Te_2$ and Measurement Conditions

Formula weight (g)	377.15
Density (calc)	7.14
$F(000)$	631
Linear absorption coefficient	228.0 cm^{-1}
Maximum correction	9.31
Minimum correction	1.31
Crystal size	$<0.12 \times 0.006 \times 0.12$ mm^3
Diffractometer	Siemens P4
Temperature	295 K
Radiation	Mo$K\alpha$
Scan mode	$\omega/(2\Theta)$
Recording range	1.00–42.50°
hklm range	$-12 < h < 12$
	$-15 < k < 26$
	$-1 < l < 7$
	$-2 < m < 2$
Standard reflections	0–42, 060, 3–21 every 100 reflections

SYMMETRY AND STRUCTURE REFINEMENT

The choice of two q vectors according to Eqs. [1] and [2] and of the basic lattice defined in Fig. 1 implies that the modulation in $NbGe_{2/5}Te_2$ is two dimensional and that the symmetry of the structure should be described by a (3 + 2)D orthorhombic superspace group. However, doubts arose on the proper symmetry of the structure because of the apparant absence of "mixed"-order satellite reflections $(h, k, l, \pm 1, \pm 1)$ or $(h, k, l, \pm 2, \pm 2)$, which may appear, for example, on the basic reciprocal axes in between the main spots. These mixed-order reflections could not be detected on long-exposure Weissenberg films or by a special search with the diffractometer on the appropriate spots in reciprocal space. Therefore, a twin model was considered with a twofold axis (twin element) along c_o^* in reciprocal space and along c in direct space. A similar model was used before by Gao *et al.* (12) to explain the complete absence of mixed-order reflections in the apparently 2D modulated structure of $Bi_2Sr_{2-x}Ca_xCuO_6$. The second q vector is related to the first q vector by the twin element; thus the modulation is no longer 2D, but is 1D. In addition, the symmetry is no longer orthorhombic, but has to be monoclinic. In princi-

ple, one can proceed with the structure analysis without any axis transformation, since a monoclinic symmetry for the modulated structure may have a basic unit cell with orthorhombic metric symmetry. To demonstrate the monoclinic symmetry more clearly, we have chosen to transform the basic unit cell according to

$$\mathbf{a}_m^* = \mathbf{a}_o^* \quad [3]$$

$$\mathbf{b}_m^* = \mathbf{b}_o^* \quad [4]$$

$$\mathbf{c}_m^* = 2\mathbf{b}_o^* + \mathbf{c}_o^*. \quad [5]$$

With this transformation, the modulation wave vector lies along the $\mathbf{c}_m^*$ axis ($\mathbf{q} = \frac{1}{5}\mathbf{c}_m^*$). As a final modification, we have taken $\mathbf{q}$ to be twice as large, since the first-order satellites match the strongest satellites. The nonstandard setting of the monoclinic space group, i.e., a-axis unique, was retained to facilitate comparison with the already published structures in the MA_xTe_2 series.

It is noted that the twin lattice, i.e., the lattice corresponding to the intersection of the lattices of the two twin components, coincides with the basic lattice of the modulated structure. One can deduce from Fig. 1 that the twin index, i.e., the ratio between the volume of the primitive unit cell of the twin components and that of the twin lattice, is five. The twin index is in this case just equal to the ratio of the volumes of supercell and basic cell.

The systematic absences of the diffraction pattern pointed to the (3 + 1)D superspace groups $P2_1/n(0\beta\gamma)$ and $P2_1/n(0\beta\gamma)0s$ (both equivalent to No. 13.1 of Table 9.8.3.5 of IT, Vol. C (13)). A few clear violations of the extinction conditions of the latter made us choose the first setting as the correct one. This was later confirmed by the refinement results. The 3D space group of this commensurate superstructure is $P2_1/n$ (a-axis unique).

The refinement of the structure was performed using the Van Smaalen–Petříček formalism for twinned structures (14). Within this formalism an extra reciprocal basic vector is used for integer indexing of all diffraction spots originating from a twinned crystal. In this case five reciprocal basic vectors ($\mathbf{a}_m^*$, $\mathbf{b}_m^*$, $\mathbf{c}_m^*$, $\mathbf{q}_1$, $\mathbf{q}_2$) are needed for integer indexing; the first three are used for the basic structure, the fourth describes the modulation, and the fifth takes into account the twinning. Using this basic set of reciprocal vectors, the matrix representation for the twin element 2_z is

$$T(2_z) = \begin{bmatrix} -1 & 0 & 0 & 0 & 0 \\ 0 & -1 & -4 & 0 & 0 \\ 0 & 0 & 1 & 0 & 0 \\ 0 & 0 & 0 & 0 & 1 \\ 0 & 0 & 0 & 1 & 0 \end{bmatrix}. \quad [6]$$

The expression for the structure factor becomes accordingly

$$F_{tw}^2(h, k, l, m_1, m_2) = (1 - \nu)F^2(h, k, l, m_1)\delta(m_2, 0) + \nu F^2(\bar{h}, \bar{k} + 4\bar{l}, m_2)\delta(m_1, 0), \quad [7]$$

where ν is the twin volume fraction and δ the Kronecker delta function which is 1.00 if both arguments are equal and 0.00 otherwise. It is noted that with this formalism the intensities of all reflections, from the overlapping reflections of the twin lattice as well as from the isolated spots, are simultaneously taken into account.

Refinement of the structure proceeded as described before (2). It was assumed that the arrangement of the cations within the sandwiches is similar to that found in $MA_{1/3}Te_2$ and $MA_{3/7}Te_2$. From this assumption starting values for the Fourier amplitudes of the occupational modulation waves were calculated and found to be in coarse agreement with the relative magnitude of the first- and second-order reflections. The refinement of the displacive modulation parameters for Te proceeded without difficulties in contrast with those for Nb and Ge where large correlations between the different parameters hampered the convergence. The reason is that some of the parameters are redundant since not all cationic positions are occupied. For example, Nb(1) occupies three independent general positions in the supercell. The symmetry allows the refinement of five parameters for each of the coordinates, i.e., the mean, and two parameters (the sine and cosine amplitude) for both the first and the second harmonic. A simple rule of thumb was developed, the so-called maximum determinant rule (15), to choose exactly those parameters which give the fewer correlations in the refinement. With this choice, the refinement converged rapidly and a false minimum could be avoided. The minimum was found to be stable against sign reversal of arbitrarily chosen Fourier amplitudes, another known pitfall in the refinement of modulated structures. In addition, a refinement was performed using the structure factor expression for incommensurate structures, since an undetected offset of the commensurate determined value of γ can produce quite different intensities at the satellite positions. It was, however, found that the R values of the commensurate calculation are much better than those of the incommensurate calculation, so it is concluded that the value for γ is exactly equal to $\frac{2}{5}$.

The final R factors are R = 0.051, 0.122, 0.187, 0.110 and wR = 0.052, 0.110, 0.181, 0.098 for main reflections, first-order satellites, second-order reflections, and main reflections, respectively. The twin volume fraction refined to 0.418(1). The parameters of the occupational waves were refined, leading to a small drop in the R factors, but the changes from 1.00 and 0.00 occupancies

TABLE 2
Final Values of the Displacive Modulation Functions for the Structure of $NbGe_{2/5}Te_2$

ν	n	$A^{\nu}_{x,s,n}$	$A^{\nu}_{y,s,n}$	$A^{\nu}_{z,s,n}$	$A^{\nu}_{x,c,n}$	$A^{\nu}_{y,c,n}$	$A^{\nu}_{z,c,n}$
Nb(1)							
	0				0.3196(3)	0.2505(4)	−0.0377(9)
	1	0.0140(6)	0.0013(4)	0.067(1)	0.0	0.0	0.0
	2	0.055(6)	0.0006(5)	0.006(1)	0.0	0.0	0.0
Nb(2)							
	0				0.0316(4)	0.2493(3)	−0.0707(8)
	1	0.0	0.0	0.0	0.0	0.0	0.0
	2	0.0	0.0	0.0	−0.0003(7)	0.0017(4)	0.030(1)
Ge							
	0				0.4236(5)	0.2494(4)	0.258(1)
	1	0.0	0.0	0.0	0.0	0.0	0.0
	2	−0.0024(7)	0.011(5)	0.031(1)	0.0	0.0	0.0
Te(1)							
	0				0.6682(2)	0.1162(1)	0.7536(4)
	1	0.0034(3)	−0.0022(2)	0.0126(6)	0.0430(3)	−0.0004(2)	0.0009(6)
	2	−0.0011(3)	−0.0002(2)	−0.0239(5)	0.0172(4)	−0.0012(2)	0.0087(6)
Te(2)							
	0				0.1678(2)	0.1159(1)	0.2124(4)
	1	−0.0448(3)	0.0003(2)	0.0094(7)	0.0062(3)	0.0018(2)	0.0203(7)
	2	−0.0087(3)	0.0034(2)	0.0356(6)	−0.0139(4)	0.0008(2)	−0.0062(7)

Note. The Fourier amplitudes of the displacive waves have been defined as

$$\mathbf{r}^{\nu}(\bar{x}_4) = \sum_{n=0}^{2} [\mathbf{u}^{\nu}_{s,n}\sin(2\pi n\bar{x}_4) + \mathbf{u}^{\nu}_{c,n}\cos(2\pi n\bar{x}_4)],$$

where ν counts the independent atoms in the basic unit cell. The argument of the modulation function has been defined as $x_4 = t + \mathbf{q}\cdot\mathbf{r}^{\nu}_{0,\mathbf{L}} = t + \mathbf{q}.(\mathbf{r}^{\nu}_0 + \mathbf{L})$, with t the global phase of the modulation wave ($t = 0$ is used in the present work), $\mathbf{L}$ a basic structure lattice translation; and $\mathbf{u}^{\nu}_{s,n} = (A^{\nu}_{x,s,n}, A^{\nu}_{y,s,n}, A^{\nu}_{z,s,n})$, $\mathbf{u}^{\nu}_{c,n} = (A^{\nu}_{x,c,n}, A^{\nu}_{y,c,n}, A^{\nu}_{z,c,n})$. It is noted that the "mean" of the modulation functions is represented by $n = 0$, but this amplitude is only equal to the crystallographic mean in the case of Te.

were only very small. Several explanations can be offered for the rather high overall agreement factors. As for all modulated structures the intensities of the satellites for this compound are rather low compared to those of the main reflections and are accordingly measured with lower accuracy. Since 77% of the data consists of satellites, this will be reflected in the overall R factors. A second explanation is offered by the uncertainty in the absorption correction due to the twinned nature of the crystal. The absorption of X-rays through the crystal depends strongly on whether microcrystals of the two different orientations are dispersed throughout the crystal, or if there are only two domains. The important role of the absorption correction is reflected in the final residues in the difference Fourier maps which are mainly found near the Te atoms, the heaviest element in the compound. However, the model resulting from the refinements is completely trustworthy, since no anomalous bond distances are found and the model scales very well with the other structures in the MA_xTe_2 series. Fourier amplitudes of the displacive modulation wave are compiled in Table 2, the (calculated) Fourier amplitudes for the occupational modulation wave in Table 3, and the final values of the temperature factors in Table 4. Lists of structure factors and tables of bond distances have been deposited.[3]

The scattering factors for neutral atoms and the anomalous dispersion correction were taken from "International Tables for X-Ray Crystallography" (16). The re-

[3] See NAPS document No. 05112 for 28 pages of supplementary material. Order from ASIS/NAPS. Microfiche Publications, P.O. Box 3513, Grand Central Station, New York, NY 10163. Remit in advance $4.00 for microfiche copy or for photocopy, $7.75 up to 20 pages plus $.30 for each additional page. All orders must be prepaid. Institutions and Organizations may order by purchase order. However, there is a billing and handling charge for this service of $15. Foreign orders add $4.50 for postage and handling, for the first 20 pages, and $1.00 for additional 10 pages of material, $1.50 for postage of any microfiche orders.

TABLE 3
Values for the Amplitudes of the Occupation Probability Modulation Waves in the Structure of $NbGe_{2/5}Te_2$[a]

n	$P^v_{s,n}$	$P^v_{c,n}$
	Nb(1)	
0		0.600000
1	−0.328786	−0.557481
2	−0.216347	−0.119618
	Nb(2)	
0		0.400000
1	0.282527	0.582292
2	0.194181	0.152997
	Ge	
0		0.400000
1	0.619499	0.187366
2	0.137006	−0.205777

[a] The values have been calculated to give a fully ordered distribution of cations, i.e., a site is empty (P = 0.00) or occupied (P = 1.00), from the defining equation

$$P^v(\bar{x}_4) = \sum_{n=0}^{2} [P^v_{s,n} \sin(2\pi n\bar{x}_4) + P^v_{c,n}\cos(2\pi n\bar{x}_4)]$$

(for the definition of the different symbols see the note to Table 2).

finements were performed in the full-matrix mode, using $w = 1/(\sigma^2(|F_{obs}|) + 0.01\,|F_{obs}|^2)$ as weights. All structural calculations have been performed with the computing system JANA93 (17).

DISCUSSION

In the MA_xTe_2 structures there are two [Te/M, A/Te] sandwiches per unit cell parallel to the **a**, **c** plane. Figure 2 shows a projection of one of the two sandwiches of $NbGe_{2/5}Te_2$ upon the plane $y = 0.25$. The Te sheets that make the sandwich are in an AA stacking mode. It is

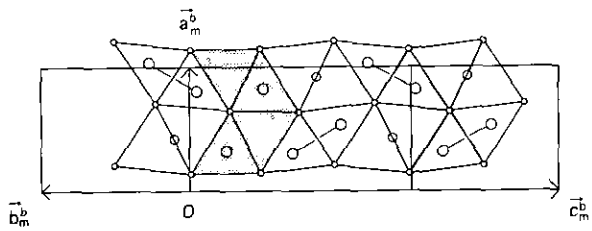

FIG. 2. Projection of one sandwich of the structure of $NbGe_{2/5}Te_2$ on the plane $y = 0.25$. Te atoms (smallest circles) form the approximate hexagonal net, Nb atoms (largest circles) are in the middle of Te triangles, and Ge atoms (medium circles) are halfway Te–Te contacts. The so-called fault is shaded.

noted that the *Pnma* symmetry of $NbGe_{1/3}Te_2$ and $NbGe_{3/7}Te_2$ requires that atoms of the second Te sheet are exactly on top of the atoms of the first sheet. This is no longer required by the $P2_1/n$ symmetry of the structure of $NbGe_{2/5}Te_2$. Nevertheless, as can be seen from Fig. 2 and a closer inspection of the data in Table 2, the exact AA stacking mode is still present to a very good approximation. In addition, the deviations of the y coordinates of the cations from 0.25, which are identical to zero in *Pnma* symmetry, are very small. These two observations imply that the m_y mirror plane, which is formally lost in going from *Pnma* to $P2_1/n$, is still approximately present. The basic structure still has approximately *Pnma* symmetry; the only significant deviation concerns the z coordinates of Te(1) and Te(2) which should sum up to 1.00 in *Pnma* symmetry.

There are four Nb–Nb pairs, two lone Nb atoms, and four Ge atoms per sandwich per unit cell in the $NbGe_{2/5}Te_2$ structure. With the general formula of the commensurate structures in the MA_xTe_2 series, viz. $MA_{(1+n)/(3+2n)}Te_2$, n = 0, 1, ... , ∞ (2), one can count $2(1 + n)$ M–M pairs per sandwich per unit cell, two lone M atoms, and $2(1 + n)A$ atoms. One peculiar feature of the MA_xTe_2 structures is the herringbone motif of M–M pairs running in the infinite two-dimensional sheets. The lone M (Nb) atoms form bands (shaded in Fig. 2) that are perpendicular to the running direction of the modulation

TABLE 4
Final Values for the Thermal Parameters[a]

	U_{11}	U_{22}	U_{33}	U_{12}	U_{13}	U_{23}
Nb(1)	0.0058(6)	0.0059(6)	0.013(1)	0.0001(9)	0.0017(7)	0.002(1)
Nb(2)	0.0054(7)	0.0047(8)	0.008(1)	0.002(1)	0.0008(7)	0.002(1)
Ge	0.010(1)	0.013(1)	0.015(1)	0.000(1)	0.000(1)	0.006(1)
Te(1)	0.0080(4)	0.0065(6)	0.0081(5)	0.0006(5)	0.0008(5)	0.0031(5)
Te(2)	0.0063(4)	0.0070(7)	0.0135(6)	0.0005(5)	0.0003(5)	0.0018(5)

[a] Temperature parameters according to the Cruickshank notation. Standard deviations in parentheses.

TABLE 5
Main Interatomic Distances in the Structures of $NbGe_{(1+n)/(3+2n)}Te_2$ (n = 0, 1, 2)[a]

Contact	$NbGe_{1/3}Te_2$				$NbGe_{2/5}Te_2$				$NbGe_{3/7}Te_2$			
	$\langle d \rangle$	$\sigma_{\langle d \rangle}$	d_{min}	d_{max}	$\langle d \rangle$	$\sigma_{\langle d \rangle}$	d_{min}	d_{max}	$\langle d \rangle$	$\sigma_{\langle d \rangle}$	d_{min}	d_{max}
Nb–Nb	2.920	0.000	2.920	2.920	2.903	0.024	2.886	2.920	2.887	0.066	2.818	2.945
Nb–Ge	2.818	0.040	2.736	2.858	2.811	0.031	2.754	2.842	2.801	0.032	2.756	2.847
Nb–Te	2.846	0.064	2.747	2.950	2.863	0.060	2.751	2.976	2.864	0.064	2.763	2.964
Ge–Te	2.768	0.026	2.745	2.790	2.777	0.030	2.735	2.820	2.770	0.032	2.728	2.800
Te–Te[b]	3.892	0.144	3.766	4.123	3.935	0.136	3.743	4.209	3.949	0.150	3.739	4.211
Te–Te[c]	3.818	0.242	3.338	4.121	3.818	0.244	3.316	4.137	3.823	0.246	3.306	4.102
Te–Te[d]	3.768	0.070	3.647	3.782	3.747	0.065	3.633	3.792	3.753	0.061	3.625	3.817

[a] $\langle d \rangle$ is the mean of all closest contacts found in the structure, $\sigma\langle d \rangle$ is the standard deviation of this mean; thus, it is not the usual crystallographic experimental standard deviation. d_{min} and d_{max} are the minimal and maximal distance, respectively, in each type of distance.

[b] Te–Te contacts through the Van der Waals gap, i.e., joining two different sandwiches.

[c] Te–Te contacts parallel through the sandwiches, i.e., within one Te sheet.

[d] Te–Te contacts through a sandwich, i.e., joining the two Te sheets that form one sandwich.

wave. Since the density of these bands of lone M atoms diminishes upon increasing n, they will be referred to as "faults," although they appear strictly periodic. Another particular feature of MA_xTe_2 structures is the square coordination of A (Ge) by Te which is not found in any other chalcogenide. A (Ge) is not only in square coordination by Te, but also approximately by Nb. Distances compare very well between the three-fold superstructure of $NbGe_{1/3}Te_2$ (n = 0), the five-fold superstructure of $NbGe_{2/5}Te_2$ (n = 1), and the seven-fold superstructure of $NbGe_{3/7}Te_2$ (n = 2) (Table 5). In addition, the standard deviations of the mean for each type of distance, and the minimum and maximum of each type, are rather similar for the three superstructures. This implies that even the individual distances do not differ much. Both Nb–Nb as Nb–Ge distances are within bonding range. The in-plane Te–Te distances have a wide range, the smallest distances (3.32 Å) being found across the Nb–Nb bonds, and the largest (4.14 Å) in the Te squares surrounding the Ge atoms.

The second sandwich within the unit cell is identical to the first sandwich, but shifted to make an overall AA/BB stacking sequence. This is true for monoclinic $NbGe_{2/5}Te_2$ as well as for orthorhombic $NbGe_{1/3}Te_2$ and $NbGe_{3/7}Te_2$. It is recalled that the basic unit cell is orthorhombic in all three cases. Figure 3 gives the relation between the orthorhombic basic unit cell and the monoclinic supercell of $NbGe_{2/5}Te_2$. It is seen that a translation along one basic vector $\mathbf{b}_o$ is accomplished by exactly two basic shifts along $\mathbf{c}_o$. This causes the cationic arrangement of the second sandwich to be in a different orientation with respect to that of the first sandwich compared to the case when the two basic shifts along $\mathbf{c}_o$ are absent (i.e., when the superstructure has orthorhombic metric symmetry). It should be noted that these two basic shifts along $\mathbf{c}_o$ do not alter the AA/BB stacking sequence.

The question as to why the monoclinic superstructure is energetically more favorable than the hypothetical orthorhombic superstructure of $NbGe_{2/5}Te_2$ is difficult to answer. It was shown before (2) by the derivation of the possible 3D space group belonging to the superspace group $Pnma(00\ n_1/n_2)s00$ that for $n_1 + n_2$ = odd, i.e., exactly for $\mathbf{q} = \frac{2}{5}\mathbf{c}^*$, a monoclinic 3D space group can be expected. One reason for the monoclinic symmetry occurrence might be the difference in relative orientation of the cationic arrangement in the two sandwiches for the monoclinic and orthorhombic variants.

Another possibility is that intersandwich Te–Te interactions cause the shift of one sandwich with respect to the other. It was shown before (2) that all structures in the MA_xTe_2 series, whether commensurate or incommensurate, can be thought to be built from three different subunits. In Fig. 4 a schematic representation is given for one sandwich for each of the three superstructures n = 0,

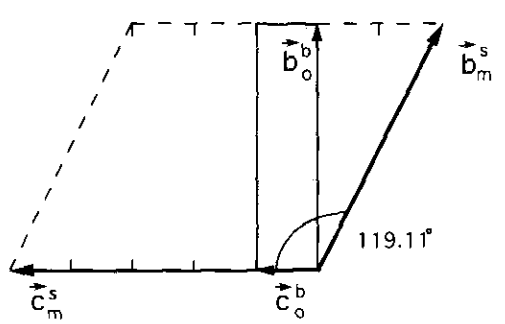

FIG. 3. Relation between the orthorhombic basic unit cell (cell axes $\mathbf{a}^b_o$, $\mathbf{b}^b_o$, $\mathbf{c}^b_o$) and the fivefold monoclinic supercell (cell axes $\mathbf{a}^s_m$, $\mathbf{b}^s_m$, $\mathbf{c}^s_m$).

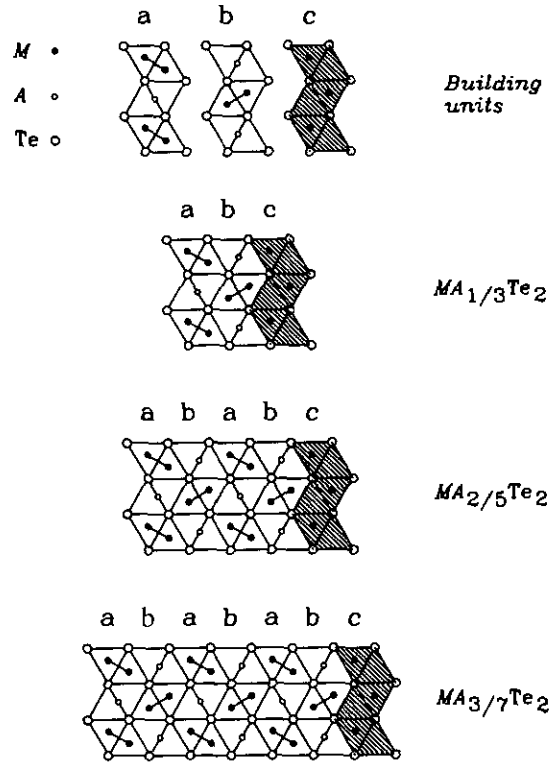

FIG. 4. Building units and structures of one sandwich of the $n = 0$, 1, 2 superstructures of $MA_{(1+n)/(3+2n)}Te_2$. The so-called fault is shaded.

1, 2. These subunits are fairly rigid, in view of the fact that the bond distances of like types for all three superstructures are rather similar (cf. Table 5). It can be easily imagined that these building blocks cannot stack in an arbitrary way if the top of each block is not flat, but buckled or puckered. In that case preferred orientations of one sheet with respect to the others will result. However, the Te sheets are nearly flat, except for two irregularities. Indeed, there are two Te atoms per sheet per unit cell[4] that are protruded slightly *inward* by roughly 0.070 Å with respect to the Te sheet. One of these atoms was also clearly visible on AFM images of the structure (9). In addition, these two atoms, one on each side of the fault, form the *shortest* contacts between the two sandwiches (3.74–3.80 Å). These short intersandwich contacts have been related to the electronic transfer from Te *p* orbitals to *M d*-block bands (3, 4). It was shown that these short contacts are essential for raising one band per sandwich, with strong Te character, above the Fermi level to adjust the oxidation state of the Te atoms. When the oxidation states of *M* and *A* are assumed to be constant throughout the $MA_{(1+n)/(3+2n)}Te_2$ series, viz. 3+ and 2+ for *M* and *A*, respectively, one calculates a mean oxidation state of $x = -(11 + 8n)/2(3 + 2n)$ for Te. In other words, 1 out of $2(3 + 2n)$ Te atoms has lost one electron. In principle, since there are exactly $2(3 + 2n)$ Te atoms per Te sheet per unit cell, only one intersandwich short Te–Te contact per Te sheet is required for the adjustment of the electron counting. Thus, the sandwich in itself is not stable, requiring short Te–Te contacts located on special positions of the Te sheets to stabilize the 3D structure. The special positions are determined by the intrasandwich geometry, and it is for that reason that the sandwiches are not stacked in an arbitrary way. Figure 5 shows the relative stacking of the two sandwiches, the special Te atoms, and the shortest intersandwich Te–Te contacts in relation with the faults.

Of course, the actual situation is more subtle: more than one intersandwich Te–Te contact per Te sheet was shown to be (slightly) bonding (3, 4), so the electron counting adjustment may be shared by several intersandwich Te–Te contacts. This is in accordance with other studies on tellurides that have shown Te anions to adopt a wide range of oxidation states between 1- and 2-, leading to a wide range of Te–Te distances (18). With regard to the monoclinic shift in $NbGe_{2/5}Te_2$, which is required to match the special positions of two adjacent Te sheets, it can be remarked that the shift is such that the relative position (counted along the *c* axis) of two faults in different sandwiches is exactly that found in the $NbGe_{1/3}Te_2$ three-fold superstructure, i.e., $\frac{3}{2} = (1 + \frac{1}{2})$ basic lattice translation along the *c* axis. For the sevenfold superstructure of $NbGe_{3/7}Te_2$ the spacing of the faults is wider, viz. $\frac{7}{2} = (3 + \frac{1}{2})$ basic lattice translation. As a more general rule, one can say that only spacings of $(k + \frac{1}{2})$, k = odd, will give the proper matching between two adjacent Te sheets needed to adjust the electron counting.

CONCLUDING REMARKS

$NbGe_{2/5}Te_2$ is a remarkable compound within the MA_xTe_2 series because of the monoclinic occupational and displacive modulation waves superimposed on an orthorhombic basic structure. Other compounds in the series have orthorhombic basic structures accompanied by orthorhombic modulation waves. The monoclinic symmetry of the modulation waves are related to a shift of exactly one basic lattice translation along $\mathbf{c}_o$ of one [Te/Nb, Ge/Te] sandwich with respect to another. A detailed analysis of bond distances and of the surface geometry of the Te sheets suggests that a sandwich can only be pinned upon another at special sites of the Te sheets, more precisely at a small number of dips in the surface. Those sites are the very ones responsible for the electronic stabilization of the structure. The dips can be made

[4] For the orthorhombic structures these two atoms are related by an *a*-glide plane.

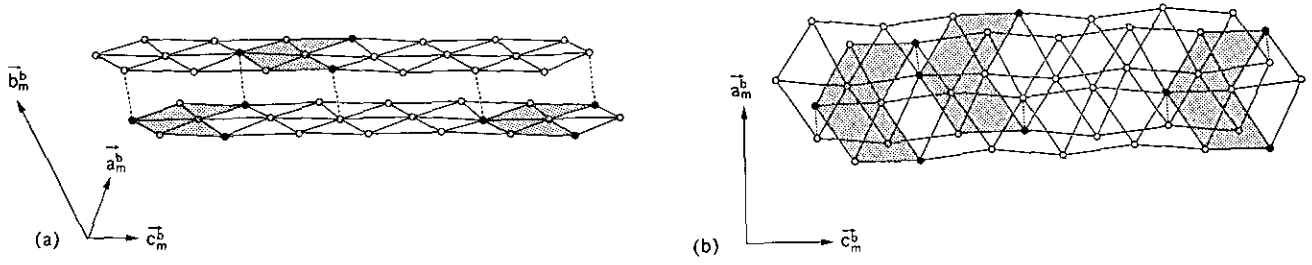

FIG. 5. Relative stacking of two consecutive sandwiches in the structure of $NbGe_{2/5}Te_2$. Shown are the two Te sheets that span the Van der Waals gap in side view (a) and in top view (b). The faults in the two sandwiches are shaded (cf. Fig. 2); closest intersandwich Te–Te contacts are indicated by hatched lines. Te atoms that are visible on AFM images are represented by small filled circles.

visible by AFM imaging (9), although their depth with respect to the otherwise flat Te sheets is only about 0.070 Å.

Of interest will be a further investigation of these dips in the surface of the Te sheets: would the electronic stabilization be absent if the dips were absent? Another question is how the pinning works in the very recently discovered incommensurate $TaSi_{0.414}Te_2$ compound with wave vector $\mathbf{q} = 0.414(1)\mathbf{c}^*$ (19). The magnitude of the wave vector of $TaSi_{0.414}Te_2$ is very close to that of $NbGe_{2/5}Te_2$, $\mathbf{q} = 0.400\mathbf{c}^*$, but in contrast with the latter compound, the former compound has orthorhombic symmetry both for its basic structure and for its modulation. The incommensurability of the $TaSi_{0.414}Te_2$ structure must be able to pin the second sandwich exactly at the right position for its electronic stabilization.

ACKNOWLEDGMENTS

The research of a.v.d.l. has been made possible by a Conseil Régional des Pays de la Loire grant and that of M.M. by NATO Grant (920049). Stimulating discussions with Dr. V. Petříček (Institute of Physics, Czech Academy of Sciences, Praha, Czech Republic) are gratefully acknowledged.

REFERENCES

1. A. van der Lee, M. Evain, L. Monconduit, R. Brec, J. Rouxel, and V. Petříček, *Acta Crystallogr. B*, **50,** 119 (1994).
2. A. van der Lee, M. Evain, L. Monconduit, R. Brec, and S. van Smaalen, *J. Phys.: Condens. Matter* **6,** 933 (1994).
3. M. Evain, L. Monconduit, A. van der Lee, R. Brec, J. Rouxel, and E. Canadell, *New J. Chem.* **18,** 215 (1994).
4. E. Canadell, L. Monconduit, M. Evain, R. Brec, J. Rouxel, and M.-H. Whangbo, *Inorg. Chem.* **32,** 10 (1993).
5. L. Monconduit, M. Evain, R. Brec, J. Rouxel, and E. Canadell, *C. R. Acad. Sci. Paris* **314,** 25 (1993).
6. J. Li and P. J. Caroll, *Mater. Res. Bull.* **27,** 1073 (1992).
7. L. Monconduit, M. Evain, F. Boucher, R. Brec, and J. Rouxel, *Z. Anorg. Allg. Chem.* **616,** 1 (1992).
8. J. Li, E. Badding, and F. J. DiSalvo, *J. Alloys Comp.* **184,** 257 (1992).
9. W. Liang, M.-H. Whangbo, M. Evain, L. Monconduit, R. Brec, H. Bengel, H. J. Cantow, and S. N. Magonov, accepted for publication, *Chem. Mater.* (1994).
10. L. Monconduit, P. Déniard, M. Evain, and R. Brec, to be published (1994).
11. S. R. Hall, H. D. Flack, and J. M. Stewart (Eds.), "Xtal3.2 Reference Manual." Universities of Western Australia, Geneva, and Maryland, 1992.
12. Y. Gao, P. Lee, J. Ye, P. Bush, V. Petříček and P. Coppens, *Physica C* **160,** 431 (1989).
13. A. J. C. Wilson (Ed.), "International Tables for Crystallography." Kluwer Academic Publishers, Dordrecht/Boston/London (1992).
14. S. van Smaalen and V. Petříček, *Acta Crystallogr. A* **48,** 610 (1992).
15. V. Petříček and A. van der Lee, in preparation (1994).
16. J. A. Ibers and W. C. Hamilton (Eds.), "International Tables for X-Ray Crystallography," Vol. IV. Kynoch, Birmingham, 1974.
17. V. Petříček, JANA93—Programs for Modulated and Composite Crystals, Institute of Physics, Praha, Czech Republic, 1993.
18. S. Jobic, R. Brec, and J. Rouxel, *J. Solid State Chem.* **96,** 169 (1992).
19. M. Evain, A. van der Lee, L. Monconduit, and V. Petříček, submitted for publication, *Chem. Mater.* (1994).